Least Squares and Marginal Log-Likelihood Model Predictive Control using Normalizing Flows

Eike Cramer[a,*]

[a] RWTH Aachen University, Process Systems Engineering (AVT.SVT), Aachen 52074, Germany

Abstract: Real-world (bio)chemical processes often exhibit stochastic dynamics with non-trivial correlations and state-dependent fluctuations. Model predictive control (MPC) often must consider these fluctuations to achieve reliable performance. However, most process models simply add stationary noise terms to a deterministic prediction. This work proposes using conditional normalizing flows as discrete-time models to learn stochastic dynamics. Normalizing flows learn the probability density function (PDF) of the states explicitly, given prior states and control inputs. In addition to standard least squares (LSQ) objectives, this work derives a marginal log-likelihood (MLL) objective based on the explicit PDF and Markov chain simulations. In a reactor study, the normalizing flow MPC reduces the setpoint error in open and closed-loop cases to half that of a nominal controller. Furthermore, the chance constraints lead to fewer constraint violations than the nominal controller. The MLL objective yields slightly more stable results than the LSQ, particularly for small scenario sets.

Keywords: Probabilistic regression; Model-free conditional probability distribution learning; Maximum log-likelihood control; Chance-constrained dynamic optimization;

1 Introduction

Model predictive control (MPC) has been established as a key technology in modern control theory and industrial application (Rawlings et al., 2017). As the name suggests, MPC requires process models to predict and optimize the process response to control inputs. While mechanistic process models are often derived as ordinary differential equations (ODEs), i.e., in continuous time format (Graham and Rawlings, 2022), MPC is often formulated for using discrete-time state space models (Rawlings et al., 2017). In their standard form, discete-time models predict the system states at the time step $\mathbf{x}[k+1]$ as a function f of the states $\mathbf{x}[k]$, the control inputs $\mathbf{u}[k]$ at the k-th time step, and system disturbance $\boldsymbol{\omega}$:

$$\begin{aligned} \mathbf{x}[k+1] &= f(\mathbf{x}[k], \mathbf{u}[k], \boldsymbol{\omega}) \\ \mathbf{x}[0] &= \mathbf{x}_0 \end{aligned} \tag{1}$$

Here, $\mathbf{x}_0$ is the initial state, and $k \in \mathbb{N}$ is a discrete number indicating the sample time $t = k\Delta t$, where Δt is the discrete time step. Such models either result from the discretization of continuous-time models or are estimated from process data. Thus, classic statistical models are some of the earliest adoptions of machine learning in chemical engineering (Söderström, 2002). Recently, machine learning models such as artificial neural networks have become popular choices of state space models with extensions to Lipschitz ANNs (Tan and Wu, 2024), physics-informed neural networks (Zheng et al., 2023), and hybrid models (Wu et al., 2020). For a review of neural networks-based process models for MPC, the reader is referred to Ren et al. (2022).

Real-world process data often exhibits a stochastic behavior, e.g., from measurement noise or disturbances. Furthermore, some processes are stochastic in nature, i.e., they exhibit inherent stochastic dynamics (Mesbah et al., 2022). This stochastic behavior requires specialized modeling tools that describe the stochastic dynamics of the process (Varshney et al., 2022). Still, most works using state space models rely on deterministic modeling, i.e., the fitted models predict only the most likely realization of the system's states. Meanwhile, stochastic process models can learn and predict the dynamics of inherently stochastic processes and quantify the impact of measurement noise on the prediction. Using stochastic process models, nominal MPC can be extended to stochastic MPC, which formulates a stochastic program (Birge and Louveaux, 2011) to minimize the expected mean and find optimal controls under uncertainty (Mesbah, 2016; Rawlings et al., 2017). In a scenario-based stochastic MPC, the stochastic process model generates scenarios of possible realizations to solve the stochastic program via sample average approximation (SAA) (Shapiro, 2009). Similarly, stochastic MPC can also be formulated using chance con-

*E. Cramer, RWTH Aachen University, Process Systems Engineering (AVT.SVT), Aachen 52074, Germany
E-mail: eike.cramer@alumni.tu-berlin.de

straints that ensure feasible control actions with a set probability (Schwarm and Nikolaou, 1999; Paulson et al., 2017). Note that control theory also knows robust MPC with guarantees for constraint satisfaction (Bemporad and Morari, 2007), but the scope of this work is restricted to the stochastic and probabilistic cases.

Most established stochastic process models use an additive, unmeasured noise term, i.e., they describe the stochastic behavior by adding a state-independent zero-mean noise term to a deterministic prediction (Box et al., 1967; Mesbah, 2016; Rawlings et al., 2017). The additive noise assumption is independent of the states, excluding any correlation between the states and the stochastic components of the dynamic response. For fermentation processes, for instance, the noise intensity varies with the cell concentration (Álvarez et al., 2018). For non-Gaussian distributions, moment-matching techniques have shown promising results, either in single dimensions (Calfa et al., 2014) or in multivariate combinations using Copulas (Bounitsis et al., 2022). These moment-matching techniques assume that the distribution is fully described by its first four statistical moments. However, stochastic MPC formulations are multi-stage decision problems requiring multistage scenarios (Ruszczyński and Shapiro, 2009), which are not naturally supported by the copula-moment-matching approach. In summary, there is a need for stochastic process models that can describe complex system behaviors, including nonlinear dynamics, potentially non-Gaussian distributions, and state-dependent stochastic dynamic response.

This work uses the deep generative model called normalizing flows (Papamakarios et al., 2021) as a probabilistic discrete-time model in the state space. Normalizing flows are flexible probability distribution models for multivariate random variables that learn explicit expressions of the probability density function (PDF) using invertible neural networks (INNs) (Papamakarios et al., 2021). The basic concept of normalizing flows can be extended to learn conditional PDFs by augmenting the INN with external inputs (Winkler et al., 2019; Rasul et al., 2021; Cramer et al., 2022b). Thus, normalizing flows also function as multivariate regression models for random variables, i.e., normalizing flows can be used as discrete-time state-space models for multivariate dynamics of systems with correlated, non-Gaussian, and state-dependent noise. Notably, normalizing flows learn high-dimensional conditional PDFs without prior assumptions and, thus, provide a highly flexible modeling architecture for stochastic processes. Hence, the control engineer does not need to have detailed knowledge about the system, its dynamics, or its stochastic behavior, as the normalizing flow can, in theory, learn any nonlinear dynamic response in combination with any probability distribution. The author has previously used normalizing flows for scenario generation of power generation time series (Cramer et al., 2022a,b) and electricity prices (Cramer et al., 2023; Hilger et al., 2024). Lu et al. (2022) present a first study investigating the temporal evolution of multivariate densities, i.e., a simulation of stochastic processes using normalizing flow similar to the method proposed in this work. Still, the most common use case for normalizing flows is image generation (Dinh et al., 2015, 2017; Grathwohl et al., 2018).

Normalizing flows sample scenarios of process realizations that can be used to solve stochastic MPC problems. Furthermore, this work shows that the explicit expression for the conditional PDF of the system states can be used to formulate a likelihood-based setpoint-tracking objective, i.e., the optimizer maximizes the likelihood that the control inputs achieve the desired setpoints. Besides the setpoint-tracking objectives, normalizing flows naturally support formulating chance constraints for any inequality constraints on the process. In summary, the contribution of this work is twofold. First, this work introduces normalizing flows as state space models for chemical processes with a particular focus on stochastic dynamics. Second, this work investigates the likelihood-based MPC objective compared to the established least squares formulation. To limit the scope of this paper, the author opts to constrain the analysis to cases where data is available in abundance or mechanistic simulations of the systems are available.

The remainder of this work is organized as follows: Section 2 reviews the basic concept of normalizing flows and their extension to conditional probability distributions. Section 3 derives the probabilistic state space formulation using the normalizing flow. Next, Section 4 reviews the least squares MPC formulation and introduces the probabilistic MPC formulation using the explicit PDF expression learned using the normalizing flow. Furthermore, the section shows how to formulate chance constraints from normalizing flow-based system simulations. Section 5 analyses the performance of the normalizing flow to predict the stochastic dynamics of an autonomous Lotka-Volterra type system. Section 6 applies the normalizing flow to learn the stochastic dynamics of a continuous stirred tank reactor (CSTR) and runs MPC in both open- and closed-loop settings. Finally, Section 7 concludes this work.

2 Normalizing Flows

This section introduces the general concept of probability density estimation using normalizing flows and reviews the extension of normalizing flows to conditional probability distributions.

2.1 Density Estimation using Normalizing Flows

Normalizing flows are explicit multivariate probability distribution models, i.e., they provide an explicit expression for the PDF $p_X(\mathbf{x})$ of a multivariate random variable X (Papamakarios et al., 2021). The random variable X is described as a diffeomorphism $T(\mathbf{z})$ of a standard Gaussian $Z \sim \phi(\mathbf{z}) = \mathcal{N}(\mathbf{0}, \boldsymbol{I})$, i.e., a bijective transformation where both forward and inverse are differentiable at least once:

$$\begin{aligned} T: \mathbb{R}^D &\rightarrow \mathbb{R}^D \\ \mathbf{z} &\mapsto T(\mathbf{z}) \end{aligned} \tag{2}$$

Here, ϕ is the standard Gaussian PDF, and Z must have the same dimensionality D as X. The diffeomorphism T describes a change of variables. Hence, the PDF of the random variable X is given by the change of variables formula (Papamakarios et al., 2021):

$$p_X(\mathbf{x}) = \phi\left(T^{-1}(\mathbf{x})\right) \left|\det \mathbf{J}_{T^{-1}}(\mathbf{x})\right| \tag{3}$$

In Equation (3), $\mathbf{J}_{T^{-1}}$ is the Jacobian matrix of the inverse of T:

$$\begin{aligned} T^{-1}: \mathbb{R}^D &\rightarrow \mathbb{R}^D \\ \mathbf{x} &\mapsto T^{-1}(\mathbf{x}) \end{aligned} \tag{4}$$

This inverse transformation projects the random variable X to a space where its counterpart Z is Gaussian. Hence, Equation (3) describes the likelihood that a data point $\mathbf{x}$ is part of the probability distribution p_X. In practice, the diffeomorphism is parameterized as an INN $\mathbf{x} = T_\Theta(\mathbf{z})$ with inverse $\mathbf{z} = T_\Theta^{-1}(\mathbf{x})$ and parameters Θ (Dinh et al., 2017). The log of Equation (3) can be used to formulate an expected log-likelihood loss function to train the parameters of the INN (Papamakarios et al., 2021):

$$\max_\Theta \mathbb{E}_X \left[\log\ p_X(\mathbf{x}; \Theta)\right] \tag{5}$$

The training then maximizes the likelihood that the inverse INN T_Θ^{-1} maps the random variable X to a standard Gaussian. To fit a normalizing flow to a dataset, i.e., a set of discrete samples $\mathbf{x}_i$ of X, the expectation in Equation (5) is substituted with its sample mean:

$$\max_\Theta \frac{1}{N} \sum_{i=1}^{N} \log\ p_X(\mathbf{x}_i; \Theta) \tag{6}$$

Here, N is the number of data points. In the following, the subscript Θ is omitted for the sake of clarity. Normalizing flows can learn the probability distribution of any multivariate continuous random variable, including multi-modal or heavily skewed probability distributions (Papamakarios et al., 2021; Dinh et al., 2017). Previous work by the author has also reported good performance on heavily tailed distributions (Cramer et al., 2023). The training via likelihood maximization is statistically consistent and asymptotically efficient (Rossi, 2018). Hence, normalizing flows converge to the correct PDF for an infinite sample size.

During training, the Jacobian determinant in Equation (3) has to be computed in every iteration, making the training prohibitively expensive for non-specialized INN architectures (Dinh et al., 2015, 2017). The most popular implementation of INNs is the real non-volume preserving transformation (RealNVP) (Dinh et al., 2017) that builds powerful transformations using compositions of partial transformations. These partial transformations are designed to yield triangular Jacobians for efficient determinant computation via the product of the diagonal entries. The author elects to omit a detailed discussion of RealNVP to avoid redundancy with existing literature. For details on the RealNVP architecture and implementation, the reader is referred to the original paper by Dinh et al. (Dinh et al., 2017), the review by Papamakarios et al. (Papamakarios et al., 2021), and the author's previous works on normalizing flows (Cramer et al., 2022a,b, 2023; Hilger et al., 2024).

2.2 Conditional Normalizing Flows

The standard form of normalizing flows discussed in Section 2.1 can be augmented by including external features. Thus, normalizing flows can also describe conditional PDFs $p_{X|Y}(\mathbf{x}|\mathbf{y})$ depending on an external feature variable Y (Winkler et al., 2019; Cramer et al., 2022b). For conditional distributions, the INN is augmented with the conditional information as additional inputs (Rasul et al., 2021;

Cramer et al., 2022b):

$$\begin{aligned} T : \mathbb{R}^D \times \mathbb{R}^M &\rightarrow \mathbb{R}^D \\ \mathbf{z}, \mathbf{y} &\mapsto T(\mathbf{z}, \mathbf{y}) \end{aligned} \tag{7}$$

Here, the dimensionality of the conditional variable Y M may be different from the data dimension D.

The conditional variable is considered as an additional input to the INN for both the forward and the inverse transformation:

$$\begin{aligned} \mathbf{x} &= T(\mathbf{z}, \mathbf{y}) \\ \mathbf{z} &= T^{-1}(\mathbf{x}, \mathbf{y}) \end{aligned}$$

Again, $\mathbf{x}$ are samples from the probability distribution the normalizing flow aims to learn, i.e., the data, $\mathbf{z}$ are samples of the multivariate standard Gaussian, and $\mathbf{y}$ is the numerical conditional information.

The change of variables described by the conditional normalizing flow remains with respect to the dimensions of the data only. The conditional information simply shapes the transformation. Thus, the change of variables reads similarly to Equation (3):

$$p_{X|Y}(\mathbf{x}|\mathbf{y}) = \phi\left(T^{-1}(\mathbf{x}, \mathbf{y})\right) |\det \mathbf{J}_{T^{-1}}(\mathbf{x}, \mathbf{y})| \tag{8}$$

Again, $\mathbf{J}_{T^{-1}}(\mathbf{x}, \mathbf{y})$ is the Jacobian with respect to $\mathbf{x}$.

After training, samples of the Gaussian can be transformed using the forward transformation to generate new data or scenarios.

$$\hat{\mathbf{x}}_{i,s} = T(\hat{\mathbf{z}}_s, \hat{\mathbf{y}}_i) \tag{9}$$

Here, the $\hat{}$ indicates new samples that are not present in the training or test sets. In the following, all normalizing flows are implemented using RealNVP with the adaptation to conditional random variables presented in Cramer et al. (2022b).

3 Probabilistic State Space Regression

This section formulates a probabilistic regression model based on the conditional normalizing flow.

Similar to Equation (1), the proposed model is written in the Markovian case, i.e., the functional relation only depends on the current time step $\mathbf{x}[k]$ and the control inputs $\mathbf{u}[k]$ at the given time step k. However, the formulation used in this work predicts the difference between states, i.e., the state increment $\mathbf{x}^{+}[k] = \mathbf{x}[k+1] - \mathbf{x}[k]$:

$$\mathbf{x}^{+}[k] \in \mathbf{F}(\mathbf{x}[k], \mathbf{u}[k]) \tag{10}$$

This work opts for the state increment vector $\mathbf{x}^{+}[k]$ over the full states $\mathbf{x}[k+1]$ to design a simpler learning problem. Equation (10) presents the difference inclusion description (Rawlings et al., 2017) of the probabilistic regression problem, where $\mathbf{F}$ is a set-valued function representing the sample space of the predicted distribution. The set described by the set-valued function $\mathbf{F}$ can be written as follows:

$$\mathbf{F} = \{f(\mathbf{x}[k], \mathbf{u}[k], \boldsymbol{\omega}) | \boldsymbol{\omega} \in \boldsymbol{\Omega}(\mathbf{x}[k], \mathbf{u}[k])\} \tag{11}$$

Opposed to typical assumptions in regression and state space models (Söderström, 2002; Rawlings et al., 2017), this work allows for state and control dependencies of the disturbances $\boldsymbol{\Omega}(\mathbf{x}[k])$ as well as non-Gaussian distributions.

In the following, Section 3.1 introduces the probabilistic state space regression using conditional normalizing flows. Section 3.2 explains the scenario generation as well as the SAA of integrals.

3.1 Probabilistic Regression using Normalizing Flows

This work uses the conditional normalizing flow to describe the probability distribution over the set-valued function in Equation (10). For the sake of brevity, the time indication $[k]$ is omitted for the remainder of this subsection.

The principle of training normalizing flows described in Section 2.1 and 2.2 translates to any combination of continuous random variables X and conditional inputs Y. Thus, normalizing flows can be used as probabilistic, multivariate regression models. For the regression in state space, the transformation is constructed to be diffeomorphic between the target variable, i.e., the state increment $\mathbf{x}^{+}$, and the Gaussian variable $\mathbf{z}$. The combination of the current states $\mathbf{x}$ and the controls $\mathbf{u}$ form the conditional information $\mathbf{y}$ in Equation (8):

$$\mathbf{x}^{+} = T_R\left(\mathbf{z}, \underbrace{[\mathbf{x}, \mathbf{u}]}_{=\mathbf{y}}\right) \tag{12}$$

Here, T_R is the INN with subscript R for regression. In practice, the state vector $\mathbf{x}$ and the controls $\mathbf{u}$ are concatenated to form a joined conditional input vector $\mathbf{y}$. Figure 2 visualizes the normalizing flow-based regression scheme for three steps. The two-headed arrows indicate the INN T_R.

Using the difference inclusion formulation (Rawlings et al., 2017), the normalizing flow-based regression model may be written analog to Equation (10):

$$\mathbf{x}^{+} \in \mathbf{T_R}(\mathbf{x}, \mathbf{u}) \tag{13}$$

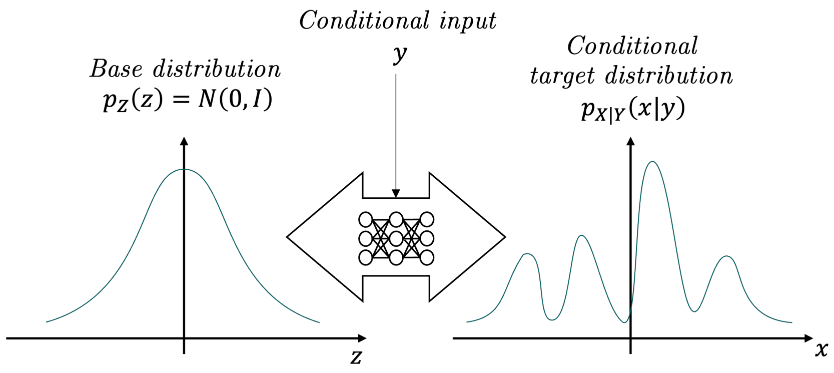

Fig. 1. Normalizing flow transformation between random variable X and Gaussian Z with conditional input variable Y. The conditional information is added to the INN as proposed in (Cramer et al., 2022b). The figure is similar to Hilger et al. (2024).

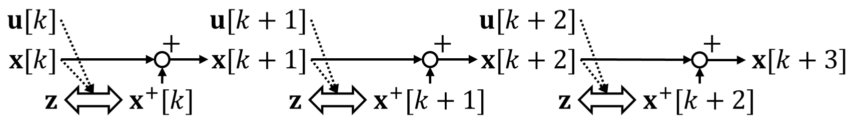

Fig. 2. Three steps of regression using normalizing flows. Here, $\mathbf{x}[k]$ are the states, $\mathbf{u}[k]$ are the control inputs, and $\mathbf{z} \sim \mathcal{N}(\mathbf{0}, \mathbb{I})$ is a multivariate Gaussian with $\dim(\mathbf{x}) = \dim(\mathbf{z})$. The two-headed arrow represents the INN T_R (Equation (12)) with conditional inputs mapping between $\mathbf{z}$ and the increment distribution $\mathbf{x}^+[k]$.

Here, $\mathbf{T_R}$ is the set of possible realizations described by the normalizing flow. The inverse of (12) reads:

$$\mathbf{z} = T_R^{-1}\left(\mathbf{x}^+, [\mathbf{x}, \mathbf{u}]\right) \tag{14}$$

Note that RealNVP (Dinh et al., 2017) requires the number of states to be ≥ 2 but poses no limitations on $\mathbf{u}$, i.e., the inputs $\mathbf{u}$ may be continuous or discrete.

The PDF of the predicted time step is again explicitly described via the change of variables formula:

$$p(\mathbf{x}^+ \,|\, [\mathbf{x}, \mathbf{u}]) = \phi\left(T_R^{-1}\left(\mathbf{x}^+, [\mathbf{x}, \mathbf{u}]\right)\right) \left|\det \mathbf{J}_{T_R^{-1}}\left(\mathbf{x}^+, [\mathbf{x}, \mathbf{u}]\right)\right| \tag{15}$$

3.2 Multistep Sampling and Integral Approximation

Equation (12) describes the general regression via the conditional normalizing flow. As the variable $\mathbf{z}$ is a random variable, the expression cannot be evaluated for the full distribution of $\mathbf{z}$. However, such evaluations are necessary to simulate the system for multiple steps or to compute integrals, e.g., over an objective. The system is written in discrete time, and the expectation over the states can be approximated via SAA over N_S scenarios $\mathbf{x}_s[k]$. Thus, the integral over a function $J(\mathbf{x}(t))$ can be approximated as follows (Asmussen and Glynn, 2007):

$$\int_0^T \mathbb{E}_{\mathbf{x}}[J(\mathbf{x}(t))]\, dt \approx \frac{\Delta t}{N_S} \sum_{k=1}^{N_T} \sum_{s=1}^{N_S} J(\mathbf{x}_s[k]) \tag{16}$$

Here, Δt is the discrete time step, and N_T is the total number of steps.

To obtain the scenarios to compute Equation (16), this work uses a Markov Chain Monte Carlo (MCMC) (Asmussen and Glynn, 2007) to compute approximations of the distribution over the states and time. Starting at an initial state, MCMC initiates N_S Markov Chains that are simulated for N_T steps. The single step prediction for scenario s in the k-th step then reads:

$$\mathbf{x}_s^+[k] = T_R(\mathbf{z}_{s,k}, [\mathbf{x}_s[k], \mathbf{u}[k]]) \tag{17}$$

In Equation (17), $\mathbf{x}_s^+[k]$ is the scenario s state increment at the k-time step, and $\mathbf{z}_{s,k}$ is a sample from the multivariate normal base distribution for scenario s and time step k. Iterating over Equation (17) yields N_S trajectories of possible scenarios that can be used to evaluate integrals as in Equation (16).

4 Model Predictive Control using Normalizing Flows

This section discusses least squares and likelihood-based state-tracking objectives for MPC based on the normalizing flow state space model. Notably, such MPC formulations with random variables present multi-stage stochastic programs, which can be difficult to formulate and solve (Shapiro, 2009). Thus, the analysis in this paper is restricted to single-stage approximations of the multi-stage stochastic programs to limit the range of this work. Hence, there are no scenario trees or recourse decisions, and all MPC formulations in this work compute a single set of control inputs $\{\mathbf{u}[k]\}_{\forall k=1,\ldots,N}$ for the considered time horizon.

The content of the section is as follows: First, Section 4.1 reviews the established formulation using the least squares objective. Second, Section 4.2 introduces an objective based on the conditional log-likelihood described by the normalizing flow. Finally, Section 4.3 shows how chance constraints can be formulated using the MCMC scenarios.

4.1 Least Squares Objective

Setpoint MPC computes the controls $\mathbf{u}$ by minimizing the predicted offset between the system setpoints $\mathbf{x}^*[k]$ and the states $\mathbf{x}[k]$ over the given time horizon $k = 1,\ldots,N_T$, where N_T is the number of time steps. The most common formulation for the objective function is the least squares (LSQ) formulation (Rawlings et al., 2017). A stochastic model yields a distribution of system realizations and, thus, stochastic MPC minimizes the expected LSQ between the states and their setpoints (Mesbah, 2016; Rawlings et al., 2017). The LSQ MPC problem using the normalizing flow $\mathbf{T_R}$ then reads:

$$\begin{aligned} \min_{\forall \mathbf{u}[k]} \quad & \sum_{k=0}^{N_T-1} \mathbb{E}\left[\Delta\mathbf{x}[k]^T \mathbf{Q} \Delta\mathbf{x}[k]\right] \Delta t \\ & \mathbf{x}^+[k] \in \mathbf{T_R}\left(\mathbf{x}[k],\mathbf{u}[k]\right) \\ \text{s.t.} \quad & \Delta\mathbf{x}[k] = \mathbf{x}^*[k] - \mathbf{x}[k] \\ & \mathbf{x}[k+1] = \mathbf{x}[k] + \mathbf{x}^+[k] \end{aligned} \tag{18}$$

Here, $\Delta\mathbf{x}[k]$ is the setpoint error at time k, and $\mathbf{Q}$ is a diagonal weight matrix. In practice, the LSQ objective in Equation (18) is intractable and instead is approximated by the expectation interval given by Equation (16).

The LSQ formulation in Equation (18) is written for the case where all states $\mathbf{x}$ have setpoints. Naturally, the formulations may be modified for cases where only a subset of the states should follow setpoints by including only those states in the formulation. In this case, the weight matrix $\mathbf{Q}$ includes zero entries on its diagonal.

4.2 Likelihood Objective

The normalizing flow-based regression model introduced in Section 3.1 gives an *explicit* expression for the conditional PDF that allows for the computation of the likelihood of the controls inducing the desired state increments. Thus, this work proposes a substitute for Equation (18) with a log-likelihood maximization. The maximum log-likelihood objective reads:

$$\begin{aligned} \max_{\forall \mathbf{u}[k]} \quad & \sum_{k=0}^{N_T-1} \mathbb{E}\left[\log p\left(\mathbf{x}^{+*}[k] | \left[\mathbf{x}[k],\mathbf{u}[k]\right]\right)\right] \Delta t \\ \text{s.t.} \quad & \mathbf{x}^{+*}[k] = \mathbf{x}^*[k+1] - \mathbf{x}[k] \end{aligned} \tag{19}$$

Here, $\mathbf{x}^{+*}[k]$ may be viewed as the perfect response achieving the setpoint in the next time step, $\mathbf{x}[k]$ are the current states, $\mathbf{u}[k]$ are the control inputs and degrees of freedom, $\mathbf{x}^*[k+1]$ are the setpoints for the next time steps, and $\log p(\cdot|\cdot,\cdot)$ is the conditional log-likelihood function described by the change of variables formula in Equation (15). Equation (19) includes the expectation operator since the current time step $\mathbf{x}[k]$ is a random variable for $k > 0$. Solving Equation (19) then maximizes the likelihood that the system takes the perfect step to the setpoints given the probability distribution described by the normalizing flow and given the respective previous states and the control inputs.

The explicit formulation of the conditional PDF in Equation 15 gives a single likelihood value for all state increments at a given time $\mathbf{x}^+[k]$. To allow for the common case of having setpoints only for a subset of the states, Equation (19) must be written for the marginal probability distribution of those states, i.e., via the marginal log-likelihood (MLL):

$$\text{MLL} = \mathbb{E}_{\mathbf{x}}\left[\int_{\mathcal{X}_j^+} \log p\left(\begin{bmatrix}\mathbf{x}_i^{+*} \\ \mathbf{x}_j^+\end{bmatrix} | \left[\mathbf{x},\mathbf{u}\right]\right) \, d\mathbf{x}_j^+\right] \tag{20}$$

Here, $\mathbf{x}_i^+$ and $\mathbf{x}_j^+$ are the state increments with and without setpoints, respectively, and $\mathcal{X}_j^+$ is the set of $\mathbf{x}_j^+$ given the current states $\mathbf{x}$ and controls $\mathbf{u}$. The time dependency $[k]$ is omitted in Equation (20) for the sake of brevity. Both Equation (19) and (20) can be approximated via the MCMC integral approximation in Equation (16) using scenarios generated from the normalizing flow. In the following, the MCMC solution of Equation (20) is referred to as the MLL objective.

4.3 Chance Constraints

Normalizing flows model the joint probability distribution of all dynamic states $\mathbf{x}[k]$ at a given time k. The knowledge of the probability distribution allows the user to formulate inequality constraints $h(\mathbf{x}[k]) \geq 0$ as chance constraints:

$$\Pr\{h(\mathbf{x}[k]) \geq 0\} \geq \varepsilon \tag{21}$$

Here, $h(\cdot)$ is the inner constraint, and ε is the probability value that should hold for satisfying the constraint. The function h might be nonlinear, and there exists no closed-form expression to implement Equation (21) into a numeric program. Instead, the chance constraint in Equation (21) can be replaced with a constraint on the corresponding quantile of the distribution of the function h:

$$p_{h(\mathbf{x}[k])}(1-\varepsilon) \geq 0 \tag{22}$$

In practice, the quantile $p_{h(\mathbf{x}[k])}(1-\varepsilon)$ is computed as an empirical quantile from evaluating h for every scenario generated using MCMC. From these scenarios, the quantile is computed via linear interpolation of the empirical inverse cumulative distribution function (CDF) (Hyndman and Fan, 1996). Note that the discrete-time formulation does not guarantee satisfying path constraints.

5 Simulation of Stochastic Autonomous Systems

This section considers the simulation of an autonomous system, namely a stochastic version of the Lotka-Volterra system (Brauer et al., 2012). The continuous time system is modeled as an SDE:

$$\begin{aligned} dX_t &= f_1(X_t,Y_t)dt + g_1(X_t,Y_t)dB_t \\ dY_t &= f_2(X_t,Y_t)dt + g_2(X_t,Y_t)dB_t \\ f_1(X_t,Y_t) &= X_t\,(\alpha - \beta Y_t) - \zeta(X_t - \bar{x}) \\ f_2(X_t,Y_t) &= X_t\,(\delta X_t - \gamma) \\ g_1(X_t,Y_t) &= \sigma X_t^{0.6} Y_t^{0.6} \\ g_2(X_t,Y_t) &= \sigma Y_t^{1.3} \end{aligned} \tag{23}$$

Here, B_t is Brownian motion. Note that the stochastic components g_1 and g_2 are nonlinear functions of the states. The parameters for the SDE are listed in Table 1. The first state drift equation f_1 includes the term $-\zeta(X_t - \bar{x})$ which corresponds to a

Tab. 1. Parameter values for the Lotka-Volterra system in Equation (23).

Parameter	Value	Parameter	Value
α	1.5	ζ	0.01
β	0.01	σ	0.01
γ	0.3	$\bar{x}$	1000
δ	$4{\cdot}10^{-4}$		

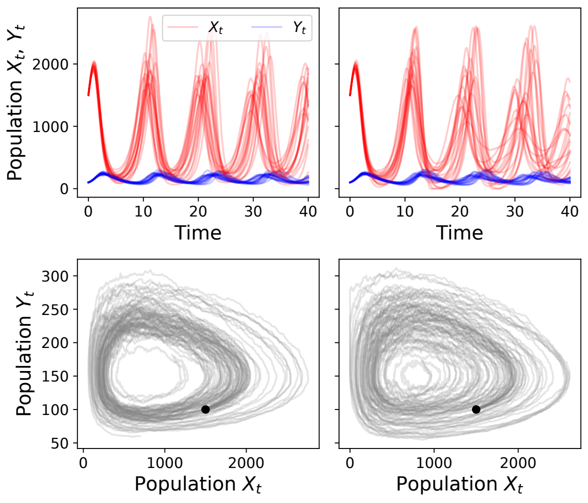

Fig. 3. Simulation of the Lotka-Volterra system (Equation (23)) with the Euler-Murayama simulation (left) and the normalizing flow simulation (right). The top row shows the populations' evolutions over time, and the bottom row shows the same in the state space. In the bottom row, the initial state is marked with a black dot.

P-control action. Without this term, the stochastic Lotka-Volterra system will result in the extinction of both species almost surely. For a detailed discussion of expectations of future system behavior, the reader is referred to Thygesen (2023).

To obtain training data for the normalizing flow, Equation System (23) is simulated using the Euler-Murayama method (Thygesen, 2023). The discrete time interval is set to $\Delta t = 0.01$ and the system is simulated for 100 periods. Note that there are multiple periods in a full revolution of the periodic repetition. The RealNVP (Dinh et al., 2017) normalizing flow is implemented using the python-based machine learning library *TensorFlow* (Abadi and Agarwal, 2015) and trained for 10 epochs using the optimizer Adam (Kingma and Ba, 2015) and a learning rate of 2×10^{-4}.

Figure 3 shows the simulation results of the

Tab. 2. Mean values μ_{ES} and standard deviation σ_{ES} of energy scores (Gneiting and Raftery, 2007) computed for the Lotka-Volterra system over 100 realizations with 200 scenarios each. Values are presented for the Euler-Murayama (EM) and the Normalizing Flow (NF) simulations.

	$N_T = 1000$		$N_T = 4000$	
	EM	NF	EM	NF
$\mu_{ES}(X_T)$	5000	5300	24000	28000
$\sigma_{ES}(X_T)$	440	450	4400	4400
$\mu_{ES}(Y_T)$	1300	1600	2100	2400
$\sigma_{ES}(Y_T)$	80	90	386	380

Euler-Murayama method (left) and the simulation using the normalizing flow (right). Starting from the initial point $(x_0, y_0)^T = (1500, 100)^T$ marked in black in the second row, the figure shows the behavior of 20 scenarios over time (top) and in the state space (bottom). Both simulations progress similarly and complete roughly four revolutions of the periodic system. The scenarios generated using the normalizing flow appear to reflect the scenarios of the Euler-Murayama solution well.

Table 2 shows a quantitative analysis using the energy score (Gneiting and Raftery, 2007). The energy score is an evaluation measure for scenario forecasts that is widely used in the forecasting literature. For a definition of the energy score, see Appendix A. While, in general, a lower energy score indicated better scenarios, the interest of this evaluation lies in reproducing the behavior of the Euler-Murayama simulation. Thus, the primary concern is whether the energy score values of the normalizing flow are similar to those of the Euler-Murayama simulation, and the absolute values in Table 2 are less significant. The energy scores of the normalizing flow are slightly higher, yet still close to the benchmark, with similar standard deviation over the 100 simulations. These results indicate good performance, particularly when considering the long simulation horizons of 1000 and 4000 time steps, respectively. In conclusion, the normalizing flow state space model learns and replicates the autonomous Lotka-Volterra system well, which is promising for further analysis of non-autonomous systems and control.

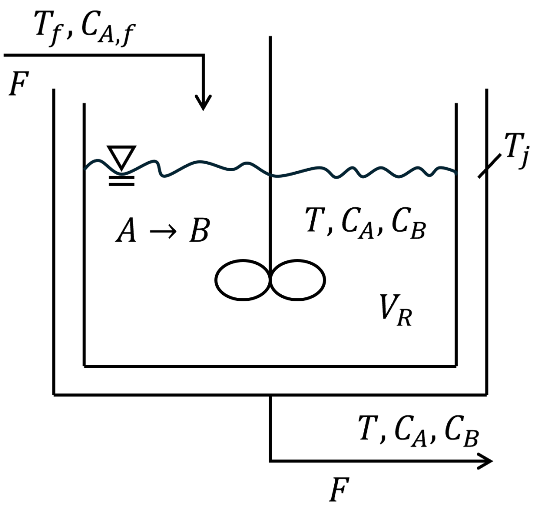

Fig. 4. Continuously stirred tank reactor (CSTR) sketch similar to Bequette (1998). State variables are the concentration of component A, C_A, and the reactor temperature T. Control variables are the feed temperature T_f, the jacket temperature T_j, and the feed concentration of component A, C_{Af}.

6 Simulation and Control of a CSTR

This section applies the normalizing flow to learn the discrete-time behavior of a CSTR and optimize the controls in open and closed-loop control settings. First, Section 6.1 introduces the case study and explains the training setup details for the normalizing flow. Next, Section 6.2 shows a probabilistic CSTR simulation. Section 6.3 shows the results of an open-loop MPC optimization using the LSQ and the MLL objective. Finally, Section 6.4 draws a comparison in closed-loop performance between the nominal benchmark MPC and the two normalizing flow MPCs.

6.1 Stochastic CSTR

The second case study in this work is the CSTR reactor model by Bequette (1998), which presents a non-autonomous system. Figure 4 shows a sketch of the process. The CSTR has two differential states: the reactor temperature T and the concentration C_A of the reagent A. The two states are controlled via three control inputs: the feed temperature T_f, the reactor jacket temperature T_j, and the concentration of the reagent A in the feed C_{Af}.

The deterministic component of the dynamics is

Tab. 3. CSTR (Bequette, 1998) parameters from MathWorks (2024).

Parameter	Value	Unit	Description
F	1	m^3/h	Volumetric flow rate
V_R	1	m^3	Reactor volume
R	1.985	kcal/(kmol·K)	Ideal gas constant
ΔH	-5,96	kcal/kmol	Heat of reaction per mole
E	11,843	kcal/kmol	Activation energy per mole
k_0	34,930,800	1/h	Pre-exponential nonthermal factor
ρC_P	500	kcal/(m^3·K)	Density multiplied by heat capacity
UA	150	kcal/(K·h)	Overall heat transfer coefficient multiplied by tank surface area

Tab. 4. CSTR control limits (Bequette, 1998).

	Min	Max
T_j [K]	273	322
T_f [K]	273	322
C_{Af} [kmol/m^3]	0	12

given by the following ODE:

$$\begin{aligned}\frac{dC_A}{dt} &= \frac{F}{V_R}(C_{Af} - C_A) - r\\ \frac{dT}{dt} &= \frac{F}{V_R}(T_f - T) - \frac{\Delta H}{\rho C_P} r - \frac{UA}{\rho C_P V_R}(T - T_j)\\ r &= k_0 C_A \exp\left(-\frac{E}{RT}\right)\end{aligned} \tag{24}$$

Here, C_A is the concentration of component A, T is the reactor temperature, T_f is the feed temperature, T_j is the jacket temperature, and C_{Af} is the feed concentration of component A. Table 3 lists the parameters and their values. The control variables and their limits are listed in Table 4.

For the experiments in this work, the CSTR is studied as a stochastic process, i.e., random events impact the dynamics of the process. Such stochastic processes are common in bio-based processes such as cell growth or fermentation (Álvarez et al., 2018). To simulate data of the stochastic process, the CSTR is extended to be an SDE, where Equation System (24) represents the drift function and the noise term is given by:

$$g(C_A, T) = \begin{bmatrix} \sigma_{C_A} C_A \\ \sigma_T |T - 270K|^{1.5} \end{bmatrix} \tag{25}$$

Notably, the noise terms have nonlinear dependence on the states, which means that the system cannot be described using standard additive noise terms. The parameter values are $\sigma_{C_A} = 0.05$ and $\sigma_T = 0.01$.

The CSTR model is simulated using the Euler-Murayama rule (Thygesen, 2023) with a discretization of 5 minutes per interval to create a dataset to train the normalizing flow. For the simulation, control inputs are randomly sampled from a uniform distribution over the control limits listed in Table 4. During the simulation, the control inputs are kept constant for 50 minutes, i.e., ten steps, for 1000 intervals. After simulation, the two states are normalized, and the controls are scaled to $[-1, 1]$ with -1 and 1 representing the minimum and maximum control actions in Table 4, respectively. The targets for the normalizing flow regression are created by computing the state increments.

The normalizing flow uses the same implementation as in Section 5, is trained for 20 epochs, and has a learning rate of 2×10^{-4}.

6.2 Simulation of CSTR

In a first analysis, this section evaluates whether the normalizing flow is able to simulate the stochastic state trajectories of the CSTR for a selection of control inputs. Figure 5 shows a simulation of the CSTR for 16 1 h intervals (12 time steps each) for randomly selected control values. The normalizing flow generates 1000 scenarios via MCMC, and the Figure shows the empirical mean values estimated by the normalizing flow (MF mean), the 50% and 99% prediction intervals, and ten realization scenarios computed via the Euler-Murayama simulation of Equation System (24) and (25). The control inputs are listed in Table 5. All simulations only receive the initial values and the controls.

The results in Figure 5 show that the normalizing flow predicts the dynamics of the stochastic CSTR well. Almost all realization scenarios are fully en-

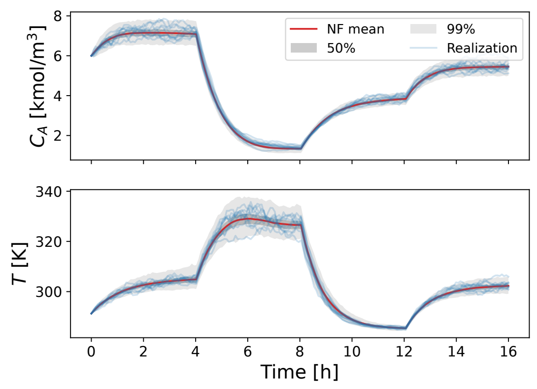

Fig. 5. Simulation of the reagent concentration C_A and the reactor temperature T for the control inputs in Table 5. The first and the second rows show the mean ("NF mean") and 50% and 99% prediction intervals for the normalizing flow in comparison to a simulation using the true model equations in (24) ("Realization"). The prediction intervals are estimated from 1000 scenarios.

Tab. 5. Control inputs to the CSTR simulation. Each input is held for four hours, i.e., 48 time steps in the 5-minute discretization.

Inputs	0-4 h	5 h-8 h	9 h-12 h	13 h-16 h
T_J [K]	300	330	270	300
T_f [K]	292	292	332	292
C_{Af} [kmol/m^3]	8	2	4	6

Tab. 6. Mean values μ_{ES} of energy scores (Gneiting and Raftery, 2007) computed for the non-autonomous CSTR system over 100 realizations with 200 scenarios each for the control inputs presented in Table 5. Values are presented for the Euler-Murayama (EM) and the Normalizing Flow (NF) simulations.

	EM	NF
$\mu_{ES}(C_A)$	2.0	2.2
$\mu_{ES}(T)$	21.6	21.7

closed within the 99% prediction intervals, and the simulation remains stable throughout the 16-hour time interval. The stability of the simulation highlights the normalizing flow's ability to learn the interaction between the noise and the drift of the dynamics of the system. Whenever noise leads to a divergence of the states, the drift is also affected as it, too, depends on the states. Notably, prediction intervals for the reactor temperature get wider for times (hours 4 to 8) when the scenarios also show higher variance. After the widening, the prediction intervals become narrower for later times (hours 8 to 12). The ability to reduce the width of the prediction intervals even for long simulation horizons underlines the ability of the normalizing flow to learn both the nonlinear drift of the dynamics and the state dependency of the fluctuations.

For a quantitative analysis, Table 6 lists the mean energy score (see Appendix A) values for the 100 realizations computed for the Euler-Murayana simulations and the normalizing flow. As discussed in Section 5, the aim of the energy score evaluation is to achieve the same values using the normalizing flow as with the Euler-Murayama, which takes the role of the ground truth. The energy score values for the simulations are very close for both the concentration C_A and the reactor temperature T.

In summary, the simulation of the stochastic CSTR confirms that the normalizing flow yields stable simulations of stochastic non-autonomous systems with accurate prediction intervals.

6.3 Open-loop MPC

This section applies the normalizing flow for open-loop MPC of the stochastic CSTR case study. The open-loop MPC solves the optimization of the LSQ formulation in Equation (18) and the MLL formulation in Equation (19) for a fixed time horizon, respectively. In every time step, the stochastic for-

Tab. 7. Setpoints for open-loop control. Each setpoint is held for 4 h, which is 48 control intervals of 5 minutes each.

Setpoints	0-4 h	5 h-8 h	9 h-12 h	13 h-16 h
C_A^* [kmol/m^3]	1.5	8	4.3	7

Tab. 8. Open-loop MPC error metrics and %-age of maximum constraint violations.

	LSQ	MLL
MAE	0.49	0.44
MSE	0.82	0.76
Violations	9.9%	7.7%

mulation is solved for 100 scenarios. The controller aims to achieve four different setpoints after each other. The four setpoints are each held for 4 h, which equals 48 time steps in the discretization to 5 minutes. The optimizer may freely manipulate the three controls for every time step within the bounds listed in Table 4. The four setpoints are listed in Table 7.

The open-loop optimization further considers a safety constraint on the reactor temperature that limits the temperature to be below 310 K. The constraint is implemented as a chance constraint with a probability of 90%:

$$Pr\{T \leq 310K\} \geq 90\% \tag{26}$$

The chance constraint is implemented via the quantile replacement discussed in Section 4.3.

Both the LSQ and MLL setpoint-tracking objective formulations are solved via the automatic differentiation wrapper in *autograd-minimize* (Rigal, 2023) and the *SLSQP* algorithm of the python-based optimization library *scipy-optimize* (Virtanen et al., 2020) in standard settings.

Figure 6 shows 20 Euler-Murayama simulations for the results of the open-loop optimization using the LSQ objective (left, blue) and the MLL objective (right, purple), respectively. In addition, the setpoints for the reactor concentration C_A^* are shown in green, and the constraint threshold on the reactor temperature is shown in red.

The figure shows that both objective formulations lead to solutions that make the controller follow the setpoints. For both objectives, the reactor concentration quickly approaches the setpoints and then continues to fluctuate with the mean on the setpoints. The profiles for LSQ and MLL objectives show very similar behavior. However, it appears that the concentration profile resulting from the MLL controls takes slightly sharper control steps for the concentration C_A, see, e.g., at the end of the first control interval at 3.5 h.

For a quantitative analysis, Table 8 lists the mean-absolute-error (MAE), the mean-squared-error (MSE), and the %-age of the maximum constraint violation for a simulation of 2000 scenarios of the solution shown in Figure 6. The results for the error metrics confirm the observations of close matches of the setpoints in Figure 6. Both MAE and MSE give low values for both objectives. Notably, the MLL objective results in slightly lower error metrics, which matches the observation of sharper control steps. The results for the maximum %-age of constraint violations further confirm that the normalizing flow-based chance constraint formulation achieves good matches of the specified probability, i.e., the controls act neither too aggressively nor too conservatively.

In 2003, Kaut and Stein (Kaut and Wallace, 2003) published their seminal work on evaluating scenario generation methods for stochastic programs. They argue that scenario generation methods should yield bias-free and stable results in the optimization. Here, bias-free means that the solution of the scenario-based program should be identical to the solution for the true distribution of the random variable. They further define stability as a low variance in the solution of the scenario-based program, even for a small number of scenarios. Kaut and Stein refer to the objective function value in the optimum as the solution to the stochastic program.

Table 9 shows statistics of the solutions to the open-loop MPC problem for different numbers of scenarios for the MCMC approximation of the LSQ objective (Equation (18)) and the MLL objective (Equation (20)) computed for 100 distinct sets of scenarios each. The mean values of the objectives for LSQ and MLL show very different values. Note that this is expected as the two functions describe different properties. Neither objective can be evaluated for the true probability distribution, as it is unknown. Hence, an analysis of the bias is not possible as intended by Kaut and Stein. For reference, the objective function values for a high number of 500 scenarios are 0.85 for the LSQ and 58.3 for the MLL objective. More important for the analysis of the stability of the solution are the higher-order statistics. The variance and kurtosis of the LSQ

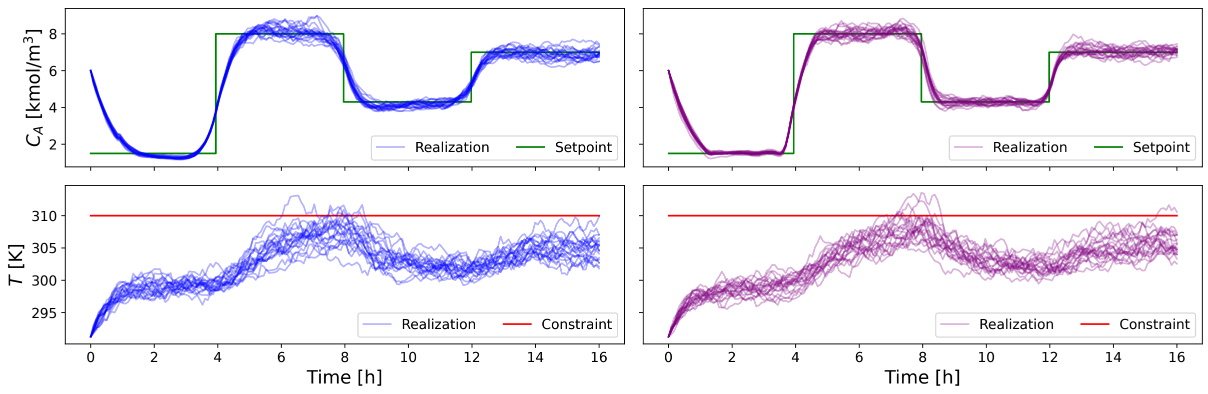

Fig. 6. Realizations of reactor concentration C_A (upper row) and reactor temperature T (lower row) for open-loop optimization using the LSQ objective (left, blue) and the MLL objective (right, purple). The setpoints are highlighted in green, and the constraint is shown in red.

Tab. 9. Results of stability analysis for LSQ and MLL objectives (Kaut and Wallace, 2003). The table shows mean values (μ), variance (σ^2), Kurtosis (KURT), and number of outliers (# Outliers) for 100 stochastic programs for different scenario set sizes.

	$S = 3$	$S = 5$	$S = 10$	$S = 20$
μ_{LSQ}	2.1	1.7	1.3	0.9
μ_{MLL}	59.4	58.2	58.1	57.6
σ^2_{LSQ}	12.7	10.3	6.4	1.7
σ^2_{MLL}	12.9	5.3	3.0	1.6
KURT$_{LSQ}$	9.3	12.3	22.9	94.5
KURT$_{MLL}$	3.4	2.6	3.6	5.1
# Outliers$_{LSQ}$	9	7	4	1
# Outliers$_{MLL}$	1	0	1	3

solutions are consistently higher compared to the MLL solution. These differences result from the higher number of outliers for the LSQ solution in all but the $S = 20$ case. The $S = 20$ case shows similar variance for both objectives, which indicates a very stable result for the MLL objective, considering the much higher mean value. The MLL objective does show more outliers for $S = 20$. However, this is likely a result of a narrow distribution, as indicated by the low kurtosis. In summary, both objectives are able to achieve stable results. However, the LSQ requires more scenarios for stability, while the MLL objective yields satisfactory stability for as few as five scenarios.

In conclusion of this analysis, the normalizing flow-based open-loop MPC achieves good results for setpoint control. Throughout the analysis of error metrics, constraint violations, and solution stability, both objective function formulations yield good results even for relatively small scenario sets. Notably, the MLL objective slightly outperforms the established LSQ objective in the error and, notably, yields more stable results for small scenario sets.

6.4 Closed-Loop MPC

Finally, this section runs the normalizing flow-based MPC in a closed-loop and draws a comparison to MPC based on the nominal model (Equation (24)). The closed-loop controllers are run with the setpoints listed in Table 7 and a prediction horizon of 2 h, i.e., 24 steps. All simulations are initialized with the same random seed to ensure comparability between the approaches. In addition to the stochastic behavior of the system in Equation (25), a measurement noise is added to the Euler Murayama simulation of the real behavior. The variance of the noise is 0.2 for the concentration and 2 for the temperature. The normalizing flow MPCs are solved using 20 scenarios.

Figure 7 shows the CSTR states and control inputs for the nominal MPC (Nominal Model) and the normalizing flow MPC using the LSQ (NF-LSQ) and the MLL (ND-MLL) objective, respectively. Note that the results only cover 14 hours, as the prediction horizon for the MPC covers the last two. Similar to the open-loop case, the normalizing flow-based controllers tightly follow the concentration setpoint profile and quickly change between setpoints. The nominal model MPC also matches all setpoints, but shows slower transitions and higher errors. Notably, the nominal MPC leads

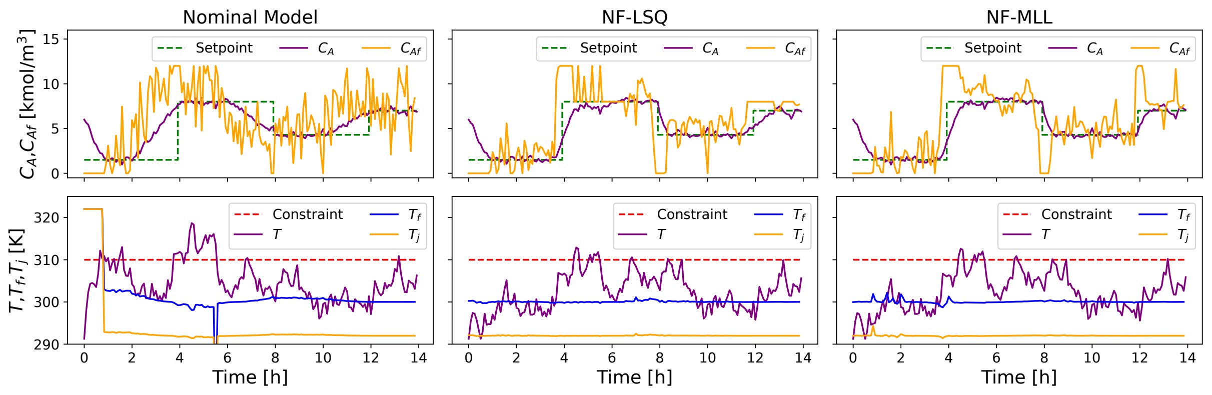

Fig. 7. Closed-loop states and controls for nominal model (Equation (24)), the LSQ objective (NF-LSQ), and the MLL objective (NF-MLL). The top column shows the concentration profiles, and the bottom column shows temperatures. The states are shown in purple, and the controls are shown in orange and blue.

to higher and more constraint violations compared to the normalizing flow controllers. This result is expected as the nominal controller does not consider the stochastic behavior of the system. The neglect of randomness in the system is also evident in the larger and more frequent control increments by the nominal controller for the feed concentration C_{Af}. The MPC formulations in this work do not penalize the control steps and, thus, the nominal controller tends to take extreme action to react to the stochastic behavior. Meanwhile, the normalizing flow state space model considers the stochastic components of the system dynamics. Hence, both LSQ and MLL objectives lead to smoother control input profiles than the nominal model. Furthermore, the normalizing flow MPCs only show minor constraint violations, as already discussed for the open-loop controller. There are only minor differences between LSQ and MLL. The MLL results show slightly fewer control jumps in the feed concentration. Meanwhile, the state profiles are almost identical, where both achieve good setpoint tracking and low constraint violations.

Table 10 shows the MAE, MSE, and the mean absolute control step (MACI) for the different closed-loop MPCs. The results for MAE and MSE confirm the observation from Figure 7 that the normalizing flow-based controllers track the setpoints better than the nominal controller. Furthermore, the MACI for the nominal controller is double that of the normalizing flow-based controllers, again, confirming the observations from above.

In summary, the normalizing flow state space model leads to good results in the closed-loop MPC and outperforms the benchmark nominal controller in all evaluations, including state tracking under uncertainty and constraint violations. Again, the MLL objective shows slightly better results than the LSO objective. However, the results for LSQ and MLL are very similar and should not be interpreted to indicate a clear superiority of the MLL objective.

Tab. 10. Mean absolute error (MAE), mean squared error (MSE), and mean absolute control increment (MACI) for the closed-loop MPC. The MACS is computed only for the feed concentration C_{Af}.

	Nominal	LSQ	MLL
MAE	1.1	0.55	0.49
MSE	3.2	0.95	0.91
MACI	2.2	1.1	1.0

7 Conclusion

This work applies the deep generative model called normalizing flows as a probabilistic state space model for chemical processes. The conditional PDF formulation of normalizing flows learns both the discrete-time stochastic dynamics with high flexibility, as there are no prior assumptions about the dynamics or their probability distribution.

This work further compares LSQ and MLL formulations of the MPC objective. Both normalizing flow-based controllers outperform the nominal test case, and the results show similar results for both formulations, with slightly better results for the MLL objective. However, the results do not support a claim for clear superiority of the MLL at this point.

Future work will investigate processes with more exotic stochastics, such as multimodal or other non-Gaussian distributions. Furthermore, analysis of the data efficiency will enhance confidence in the usability of the normalizing flow-based MPC for practical applications with limited data.

A Energy Score

This work uses the energy score (Gneiting et al., 2008; Pinson and Girard, 2012) to assess the quality of the normalizing flow scenarios. The energy score is defined as follows

$$\begin{aligned}\mathrm{ES}[k] =& \frac{1}{N_S}\sum_{s=1}^{N_S} ||\mathbf{x}[k] - \hat{\mathbf{x}}_s[k]||_2 \\ &- \frac{1}{2{N_S}^2}\sum_{s=1}^{N_S}\sum_{s'=1}^{N_S} ||\hat{\mathbf{x}}_s[k] - \hat{\mathbf{x}}_{s'}[k]||_2\end{aligned} \tag{27}$$

Here, $\mathbf{x}$ is the realized state vector and $\hat{\mathbf{x}}_s$ are sample vectors generated using MCMC, N_S is the number of samples, and $||\cdot||_2$ is the 2-norm.

Bibliography

Abadi, M. and Agarwal, A. (2015). TensorFlow: Large-scale machine learning on heterogeneous systems. https://www.tensorflow.org/. Accessed on 08-08-2022.

Asmussen, S. and Glynn, P. W. (2007). *Stochastic Simulation: Algorithms and Analysis*. Springer New York.

Bemporad, A. and Morari, M. (2007). *Robust Model Predictive Control: A Survey*, page 207–226. Springer London.

Bequette, B. W. (1998). Process dynamics: modeling, analysis, and simulation. Lecture notes.

Birge, J. R. and Louveaux, F. (2011). *Introduction to stochastic programming*. Springer Science & Business Media, New York, US.

Bounitsis, G. L., Papageorgiou, L. G., and Charitopoulos, V. M. (2022). Data-driven scenario generation for two-stage stochastic programming. *Chemical Engineering Research and Design*, 187:206–224.

Box, G. E., Jenkins, G. M., and Bacon, D. W. (1967). Models for forecasting seasonal and non-seasonal time series. Technical report, Wisconsin Univ. Madison Department of Statistics.

Brauer, F., Castillo-Chavez, C., and Castillo-Chavez, C. (2012). *Mathematical models in population biology and epidemiology*, volume 2. Springer.

Calfa, B., Agarwal, A., Grossmann, I., and Wassick, J. (2014). Data-driven multi-stage scenario tree generation via statistical property and distribution matching. *Computers & Chemical Engineering*, 68:7–23.

Cramer, E., Mitsos, A., Tempone, R., and Dahmen, M. (2022a). Principal component density estimation for scenario generation using normalizing flows. *Data-Centric Engineering*, 3:e7.

Cramer, E., Paeleke, L., Mitsos, A., and Dahmen, M. (2022b). Normalizing flow-based day-ahead wind power scenario generation for profitable and reliable delivery commitments by wind farm operators. *Computers & Chemical Engineering*, 166:107923.

Cramer, E., Witthaut, D., Mitsos, A., and Dahmen, M. (2023). Multivariate probabilistic forecasting of intraday electricity prices using normalizing flows. *Applied Energy*, 346:121370.

Dinh, L., Krueger, D., and Bengio, Y. (2015). NICE: Non-linear independent components estimation. In Bengio, Y. and LeCun, Y., editors, *3rd International Conference on Learning Representations, ICLR 2015, San Diego, CA, USA, May 7-9, 2015, Workshop Track Proceedings*.

Dinh, L., Sohl-Dickstein, J., and Bengio, S. (2017). Density estimation using Real NVP. In *5th International Conference on Learning Representations, ICLR 2017, Toulon, France, April 24-26, 2017, Conference Track Proceedings*. OpenReview.net.

Gneiting, T. and Raftery, A. E. (2007). Strictly proper scoring rules, prediction, and estimation. *Journal of the American Statistical Association*, 102(477):359–378.

Gneiting, T., Stanberry, L. I., Grimit, E. P., Held, L., and Johnson, N. A. (2008). Assessing probabilistic forecasts of multivariate quantities, with an application to ensemble predictions of surface winds. *Test*, 17(2):211–235.

Graham, M. D. and Rawlings, J. B. (2022). *Modeling and analysis principles for chemical and biological engineers*. Nob Hill Publishing.

Grathwohl, W., Chen, R. T. Q., Bettencourt, J., Sutskever, I., and Duvenaud, D. (2018). FFJORD: free-form continuous dynamics for scalable reversible generative models. *CoRR*, abs/1810.01367.

Hilger, H., Witthaut, D., Dahmen, M., Rydin Gorjão, L., Trebbien, J., and Cramer, E. (2024). Multivariate scenario generation of day-ahead electricity prices using normalizing flows. *Applied Energy*, 367:123241.

Hyndman, R. J. and Fan, Y. (1996). Sample quantiles in statistical packages. *The American Statistician*, 50(4):361–365.

Kaut, M. and Wallace, S. W. (2003). *Evaluation of scenario-generation methods for stochastic programming*. Humboldt-Universität zu Berlin, Mathematisch-Naturwissenschaftliche Fakultät II, Institut für Mathematik, Berlin, Germany.

Kingma, D. P. and Ba, J. (2015). Adam: A method for stochastic optimization. In Bengio, Y. and LeCun, Y., editors, *3rd International Conference on Learning Representations, ICLR 2015, San Diego, CA, USA, May 7-9, 2015, Conference Track Proceedings*, pages 1–11.

Lu, Y., Maulik, R., Gao, T., Dietrich, F., Kevrekidis, I. G., and Duan, J. (2022). Learning the temporal evolution of multivariate densities via normalizing flows. *Chaos: An Interdisciplinary Journal of Nonlinear Science*, 32(3).

MathWorks (2024). Time series. `https://de.mathworks.com/help/mpc/gs/cstr-model.html`. Accessed: 2024-04-23.

Mesbah, A. (2016). Stochastic model predictive control: An overview and perspectives for future research. *IEEE Control Systems*, 36(6):30–44.

Mesbah, A., Wabersich, K. P., Schoellig, A. P., Zeilinger, M. N., Lucia, S., Badgwell, T. A., and Paulson, J. A. (2022). Fusion of machine learning and mpc under uncertainty: What advances are on the horizon? In *2022 American Control Conference (ACC)*. IEEE.

Papamakarios, G., Nalisnick, E., Rezende, D. J., Mohamed, S., and Lakshminarayanan, B. (2021). Normalizing flows for probabilistic modeling and inference. *Journal of Machine Learning Research*, 22(57):1–64.

Paulson, J. A., Buehler, E. A., Braatz, R. D., and Mesbah, A. (2017). Stochastic model predictive control with joint chance constraints. *International Journal of Control*, 93(1):126–139.

Pinson, P. and Girard, R. (2012). Evaluating the quality of scenarios of short-term wind power generation. *Applied Energy*, 96:12–20.

Rasul, K., Sheikh, A.-S., Schuster, I., Bergmann, U. M., and Vollgraf, R. (2021). Multivariate probabilistic time series forecasting via conditioned normalizing flows. In *International Conference on Learning Representations*, Vienna, Austria.

Rawlings, J. B., Mayne, D. Q., Diehl, M., et al. (2017). *Model predictive control: theory, computation, and design*, volume 2. Nob Hill Publishing Madison, WI.

Ren, Y. M., Alhajeri, M. S., Luo, J., Chen, S., Abdullah, F., Wu, Z., and Christofides, P. D. (2022). A tutorial review of neural network modeling approaches for model predictive control. *Computers & Chemical Engineering*, 165:107956.

Rigal, B. (2023). autograd-minimize. https://github.com/brunorigal/autograd-minimize.

Rossi, R. J. (2018). *Mathematical statistics: An introduction to likelihood based inference*. John Wiley & Sons.

Ruszczyński, A. and Shapiro, A. (2009). *3. Multistage Problems*, page 63–85. Society for Industrial and Applied Mathematics.

Schwarm, A. T. and Nikolaou, M. (1999). Chance-constrained model predictive control. *AIChE Journal*, 45(8):1743–1752.

Shapiro, A. (2009). *5. Statistical Inference*, page 155–252. Society for Industrial and Applied Mathematics.

Söderström, T. (2002). *Discrete-time Stochastic Systems: Estimation and Control*. Springer London.

Tan, W. G. Y. and Wu, Z. (2024). Robust machine learning modeling for predictive control using lipschitz-constrained neural networks. *Computers & Chemical Engineering*, 180:108466.

Thygesen, U. H. (2023). *Stochastic Differential Equations for Science and Engineering.* Chapman and Hall/CRC.

Varshney, D., Patwardhan, S. C., Bhushan, M., and Biegler, L. T. (2022). Moving horizon estimator for nonlinear and non-gaussian stochastic disturbances. *Journal of Process Control*, 116:234–254.

Virtanen, P., Gommers, R., Oliphant, T. E., Haberland, M., Reddy, T., Cournapeau, D., Burovski, E., Peterson, P., Weckesser, W., Bright, J., van der Walt, S. J., Brett, M., Wilson, J., Millman, K. J., Mayorov, N., Nelson, A. R. J., Jones, E., Kern, R., Larson, E., Carey, C. J., Polat, İ., Feng, Y., Moore, E. W., VanderPlas, J., Laxalde, D., Perktold, J., Cimrman, R., Henriksen, I., Quintero, E. A., Harris, C. R., Archibald, A. M., Ribeiro, A. H., Pedregosa, F., van Mulbregt, P., and SciPy 1.0 Contributors (2020). SciPy 1.0: Fundamental Algorithms for Scientific Computing in Python. *Nature Methods*, 17:261–272.

Winkler, C., Worrall, D., Hoogeboom, E., and Welling, M. (2019). Learning likelihoods with conditional normalizing flows. *arXiv preprint arXiv:1912.00042*.

Wu, Z., Rincon, D., and Christofides, P. D. (2020). Process structure-based recurrent neural network modeling for model predictive control of nonlinear processes. *Journal of Process Control*, 89:74–84.

Zheng, Y., Hu, C., Wang, X., and Wu, Z. (2023). Physics-informed recurrent neural network modeling for predictive control of nonlinear processes. *Journal of Process Control*, 128:103005.

Álvarez, J., Baratti, R., Tronci, S., Grosso, M., and Schaum, A. (2018). Global-nonlinear stochastic dynamics of a class of two-state two-parameter non-isothermal continuous stirred tank reactors. *Journal of Process Control*, 72:1–16.